Check for updates

ADVANCED HEALTHCARE MATERIALS
www.advhealthmat.de

Cationic Tricyclic AIEgens for Concomitant Bacterial Discrimination and Inhibition

Bingnan Wang, Haozhong Wu, Rong Hu, Xiaolin Liu, Zhiyang Liu, Zhiming Wang, Anjun Qin, and Ben Zhong Tang**

New ionic compounds with aggregation-induced emission (AIE) feature has been widely studied. These AIE-based luminogens (AIEgens) not only effectively resolve aggregation-caused quenching (ACQ) problems that are encountered for most of conventional fluorescent dyes, but also exhibit promising applications in biological imaging, potentially for a wide variety of diseases. However, such an AIE system needs to be further developed. In this work, a series of novel cationic AIEgens that are comprised of tricyclic 2-aminopyridinium derivatives with seven-membered rings are designed and synthesized via a simple, multicomponent reaction. Notably, these AIEgens exhibit the ability to specifically stain gram-positive bacteria. Moreover, a specific AIEgen, BMTAP-7, possesses highly efficient bacteriostatic ability for *Staphylococcus aureus* (*S. aureus*) in both liquid medium and solid agar plates, which have a minimum inhibitory concentration (MIC) between 4 and 8 μg mL^{-1}. Using live-cell imaging and a wash-free process, it is observed that hydrophilic AIEgens are localized to mitochondria, whereas lipophilic AIEgens display specific staining of lysosomes. These AIEgens with bacteriostatic activity hold great promise for distinguishing between bacterial types and inhibiting bacterial infections in situ.

1. Introduction

Bacterial infections can cause serious illnesses, such as dermatosis, pneumonia, and septic arthritis, which have increasingly raised and threatened public health.[1] Reliably and rapidly diagnosing as well as finding effective therapies against bacterial infections are two key components that are of interest in clinical research.[2] However, drug-resistant bacteria have generated due to the overuse of antibiotics in the therapeutic process. For example, gram-positive, methicillin-resistant *Staphylococcus aureus* (*S. aureus*) (MRSA) is resistant to multiple antibiotics and causes common infectious diseases in hospitals.[3] Therefore, it is of great significance for pharmacology and biomedicine research to develop new bactericidal and bacteriostatic agents.

Diagnosing bacterial infections are required for effective and precise treatments. At present, the traditional Gram-staining method is used for distinguishing gram-positive and gram-negative bacteria; however, the Gram-staining process is extremely complicated, requiring varied reagents and multiple washing, and the in situ detection of living bacteria is impossible. Other generally adopted methods for bacterial identification include gene microarrays,[4] immunological analysis,[5] polymerase chain reactions,[6] and biochemical sensing,[7] but these techniques are time consuming, complex in operation, and require sophisticated instruments. To overcome these shortcomings, new methods that could quickly and accurately identify bacteria are essential.

Recently, fluorescence technology has been rapidly developed and applied in bacterial identification,[8] because of its remarkable simplistic advantages and superior sensitivity.[9] However, the majority of traditional fluorescent materials are lipophilic and tend to aggregate in the biological aqueous environment, thereby inducing the aggregation-caused quenching (ACQ) effect. As a consequence of this effect, the fluorescence intensity is quenched or weakened in the aggregate state or at high concentrations. The ACQ effect confines the operating levels of traditional fluorescent materials to lower concentrations and limits long-term tracking due to degrees of labeling, which in turn restricts their applications in biological imaging, accurately diagnosing, and photodynamic antibacterial therapy.[10]

Aggregation-induced emission (AIE), an opposing phenomenon to the conventional ACQ effect, was proposed by our group in 2001, which shows stronger emissions from aggregated luminogens than those in solution.[11] To date, multifarious AIEgens have been synthesized under the mechanism of

B. Wang, H. Wu, Dr. R. Hu, Prof. Z. Wang, Prof. A. Qin, Prof. B. Z. Tang
State Key Laboratory of Luminescent Materials and Devices
Guangdong Provincial Key Laboratory of Luminescence from Molecular Aggregates
SCUT-HKUST Joint Research Institute
Center for Aggregation-Induced Emission
South China University of Technology (SCUT)
Guangzhou 510640, China
E-mail: msqinaj@scut.edu.cn; tangbenz@ust.hk
X. Liu, Dr. Z. Liu, Prof. B. Z. Tang
Department of Chemistry
Hong Kong Branch of Chinese National Engineering Research Centre for Tissue Restoration and Reconstruction
Institute for Advanced Study
and Department of Chemical and Biological Engineering
The Hong Kong University of Science & Technology (HKUST)
Clear Water Bay, Kowloon, Hong Kong, China

The ORCID identification number(s) for the author(s) of this article can be found under https://doi.org/10.1002/adhm.202100136

DOI: 10.1002/adhm.202100136

 © 2021 Wiley-VCH GmbH

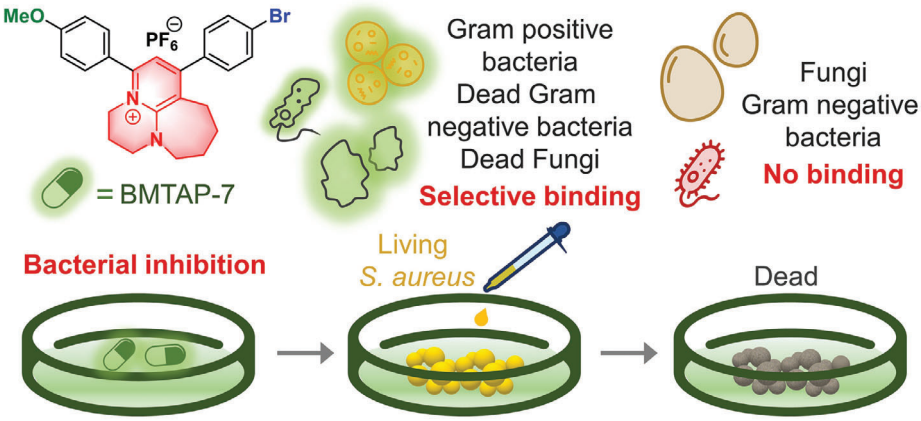

Figure 1. Illustration of specific discrimination and inhibition for microorganism by BMTAP-7.

restriction of intramolecular motion (RIM) that guide the AIE effect, which includes restriction of intramolecular rotation (RIR) and restriction of intramolecular vibration (RIV). It is worth mentioning that using cationic AIEgens as the main component have been developed for bioimaging, biosensing, biological diagnosis, and treatment.[12] Owing to their admirable characteristics, cationic AIEgens have high quantum yields in the aggregate state, good water solubility, large Stokes shift, turn-on features in bioassays, high signal-to-noise ratio, and elevated photostability.[13]

However, there are some potential issues that need to be addressed. In terms of water-soluble elements, cationic AIEgens are mainly comprised of pyridine, triphenyl phosphorous, and quaternary ammonium salts,[14] which are not easily separated via column chromatography, particularly when modifying their structures. Notably, most of the AIEgens were synthesized according to the RIR mechanism, but few functional groups have also been modified using the RIV mechanism.[11] Excitingly, the AIEgens have been widely applied in diverse areas, including bacterial discrimination.[15] However, the AIEgens with the capacity to discriminate and have pharmacologic activity for bacteria have been rarely reported.

Therefore, we synthesized a series of cationic tricyclic 2-aminopyridinium derivatives with 1,8-diazabicyclo[5.4.0]undec-7-ene (DBU), an organic base commonly used in organic chemistry and a functional group followed the RIV mechanism.[16] Meanwhile, the photophysical properties, theoretical calculations, and organelle-specific imaging of the synthetic tricyclic 2-aminopyridinium derivatives, and their ability for bacterial discrimination and inhibition were characterized (**Figure 1**). Furthermore, we explored the bacteriostatic mechanism using a control experiment to find possible targets. This study not only provides novel cationic AIEgens that could discriminate and inhibit bacteria, but also promotes the development of bacteriostatic materials.

2. Results and Discussion

2.1. Design and Synthesis of AIEgens

Compounds BMTAPC-5, BMTAPC-7, BMTAP-7, TMTAP-7, and DTTAP-7, whose structures are shown in **Figure 2**A, were designed. These compounds are composed of tricyclic 2-aminopyridinium moiety as the electron acceptor, methoxyl group, and/or triphenylamine (TPA) as an electron donor. In addition, the bromo and methoxyl groups might show high hydrophilicity to facilitate bio-related applications. As a result, they demonstrated donor–π-acceptor structures, which readily changed their conjugated length. For BMTAPC-5 and BMTAPC-7, when the five- and seven-membered rings are introduced into the two molecules, respectively, their luminescent properties are dramatically different in both solutions and solid states.[46] Moreover, the positively charged tricyclic 2-aminopyridinium moiety not only acts as an electron acceptor, but also potentially endows the AIEgens to be applied to negatively-charged bacteria during imaging and exert antibacterial activity.[18] For BMTAP-7, TMTAP-7, and DTTAP-7, the TPA segments were gradually added to the molecular structures as electron-donating groups, which affected their luminescent properties and hydrophilicity. These compounds could be facilely synthesized by simple organic reactions as previously reported.[17] Experimental procedures and structural characterization data are provided in the Supporting Information.

2.2. Photophysical Properties

After confirming their structures, the photophysical properties of these five compounds were investigated. Figure 2B–D shows the UV/Vis absorption and photoluminescence (PL) spectra in their different states for each compound, and **Table 1** summarizes the corresponding data. The absorption peak (λ_{abs}) of BMTAPC-7 at 361 nm is close to that of BMTAPC-5 (359 nm) in a dilute dichloromethane (DCM) solution. TMTAP-7 showed a slightly red-shifted absorption peak (λ_{abs}, 365 nm) compared with those of BMTAP-7 and DTTAP-7 (360 nm) in a dilute tetrahydrofuran (THF) solutions (Figure 2B). From the PL spectra of the compounds in solid states (Figure 2C), we observed that BMTAP-7 displayed an emission peak at 469 nm, whereas those for BMTAPC-5 and BMTAPC-7 were 493 nm. In contrast, TMTAP-7 and DTTAP-7 showed redder emission peaks at 534 and 550 nm, respectively. The shift was likely caused by adding TPA segments to increase the molecular conjugation of the luminophores. In solutions, these five compounds emitted similar wavelengths

© 2021 Wiley-VCH GmbH

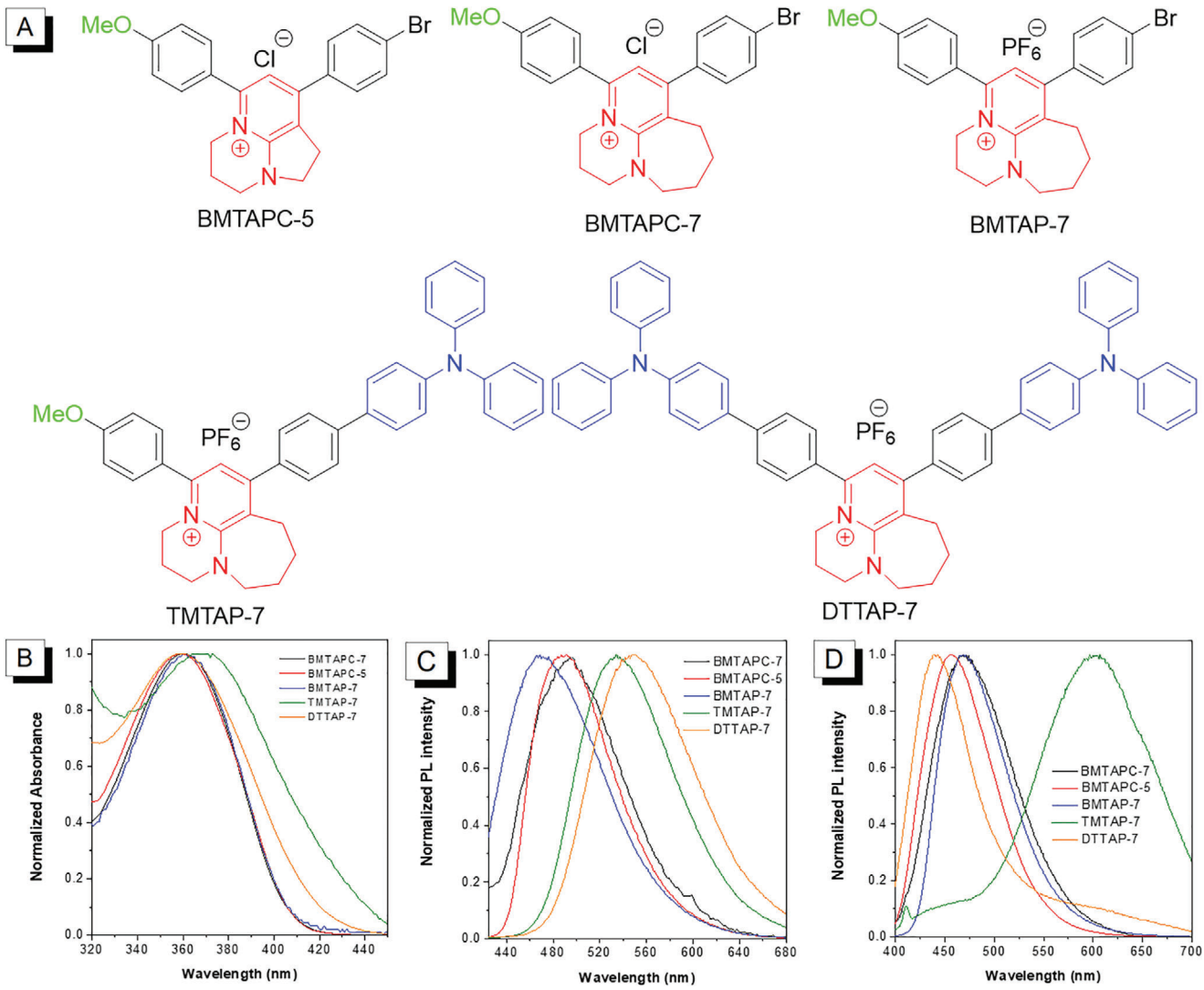

Figure 2. A) Molecular structures of the designed materials. B) Normalized absorption spectra of BMTAPC-5, BMTAPC-7, BMTAP-7, TMTAP-7, and DTTAP-7 dissolved in dichloromethane (DCM) or tetrahydrofuran (THF) solutions. C) Normalized PL spectra of five molecules in solid. D) Normalized PL spectra of BMTAPC-5, BMTAPC-7, BMTAP-7, TMTAP-7, and DTTAP-7 in DCM or THF solutions.

Table 1. Photophysical properties of five compounds.

	λ_{abs} [nm]	λ_{em} [nm]		Φ_F [%]		τ [ns]	
	soln	soln	solid film	soln	solid film	soln	solid film
BMTAPC-7	361[a)]	471	494	3.5	21.7	0.7	3.0
BMTAPC-5	359	457	492	31.3	1.6	2.4	1.3
BMTAP-7	361	469	469	3.4	28.5	0.8	4.1
TMTAP-7	365	450/607	534	8.3	16.5	0.9	16.4
DTTAP-7	360	603	550	5.0	10.2	2.0	13.6

[a)] Photophysical properties of BMTAPC-7 and BMTAPC-5 were tested in DCM solution, and BMTAP-7, TMTAP-7, and DTTAP-7 were tested in THF solution.

from 400 to 500 nm; however, TMTAP-7 and DTTAP-7 exhibited longer wavelength emission at approximately 607 and 603 nm (Figure 2D), respectively. The differences in the absorption and emission peaks among the compounds were probably due to their different conjugations and intramolecular charge transfer process.

Subsequently, the PL spectra of BMTAPC-5 and BMTAPC-7 in the DCM/*n*-hexane mixtures with different *n*-hexane fractions (f_hs) were measured (Figure S1, Supporting Information; Table 1). Notably, both BMTAPC-5 and BMTAPC-7 were more soluble in the DCM solution and could not be dissolved in the *n*-hexane mixtures. When the f_h was 99%, the PL intensity for BMTAPC-7 increased sharply, whereas the PL intensity for BMTAPC-5 decreased even with an increase in the f_h. This phenomenon occurred because the molecules form aggregates with high f_hs, which limits intramolecular seven-membered ring vibrations and leads to an enhancement of PL intensity.[16] The absolute PL quantum yield (Φ_F) measurement further confirmed the above phenomena. As shown in Table 1, BMTAPC-7 showed a lower Φ_F value of 3.5% in the DCM solution than that (21.7%)

© 2021 Wiley-VCH GmbH

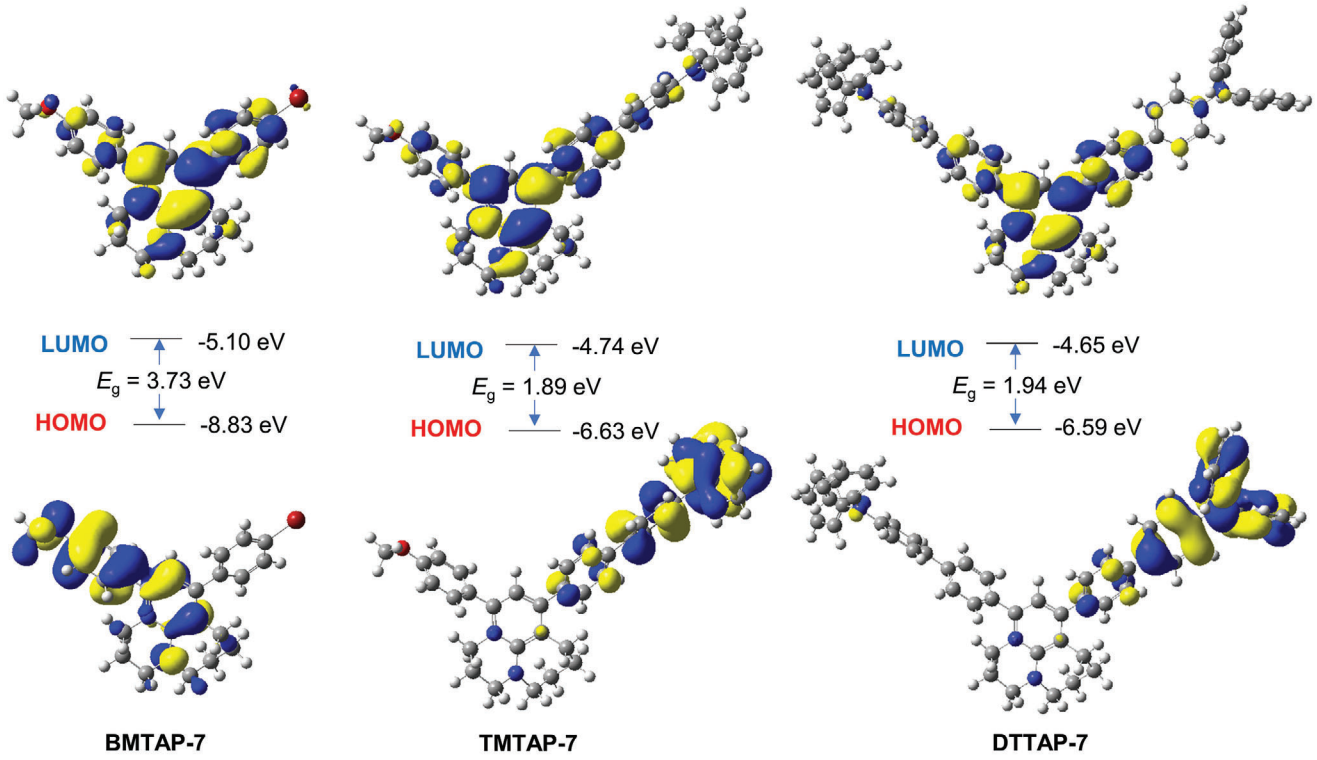

Figure 3. Molecular orbital amplitude plots of HOMOs and LUMOs energy levels of BMTAP-7, TMTAP-7, and DTTAP-7 in a cationic state calculated using the B3LYP/6-31G** level.

in the solid film, whereas BMTAPC-5 showed a higher Φ_F value of 31.3% in the DCM solution than that (1.6%) in the solid film. These results demonstrate that the main reason behind the AIE phenomenon is that intramolecular seven-membered ring vibrations are restricted in the solid or aggregate state.

Thanks to their donor-π-acceptor structures, TMTAP-7 and DTTAP-7 exhibited observable solvatochromic effects. The PL intensity decreased with increasing solvent polarity, and significantly enhanced with in low polar solutions (Figure S2, Supporting Information). These results suggest that the DCM/*n*-hexane system might not be suitable for testing the AIE feature of these compounds. Therefore, we changed the solvent mixture to THF/water. As shown in Figure S1 (Supporting Information) and Table 1, the AIE effects for BMTAP-7, TMTAP-7, and DTTAP-7 were activated in the THF/water mixtures that contained high water fractions. Moreover, these compounds displayed higher Φ_F values in the solid state than those in the THF solutions. Additionally, the PL lifetime measurements revealed that these seven-membered ring AIEgens have a longer lifetime in the solid state than in solutions (Table 1) because the nonradiative transition is limited in solid states.[16]

2.3. Theoretical Calculations

To better understand the distinctions among the photophysical properties, BMTAP-7, TMTAP-7, and DTTAP-7 were further investigated via density functional theory (DFT) calculations. The geometries of BMTAP-7, TMTAP-7, and DTTAP-7 were optimized using the B3LYP/6-31G** level (**Figure 3**). The highest occupied molecular orbitals (HOMOs) of these AIEgens were mainly localized at the TPA moiety or 4-methoxyphenyl group, whereas their lowest unoccupied molecular orbitals (LUMOs) were distributed throughout the tricyclic 2-aminopyridinium or whole molecules. Moreover, the calculated HOMO–LUMO energy gaps of TMTAP-7 and DTTAP-7 were smaller than those of BMTAP-7 owing to the stronger electron donor–acceptor-based interactions between TPA and tricyclic 2-aminopyridinium, which also corresponded to the redder emission peaks.

2.4. In Vitro Fluorescence Imaging

For bio-related applications of a probe, its biocompatible is a key issue. Thus, we tested the cytotoxicity of BMTAP-7, TMTAP-7, and DTTAP-7 using a standard MTT test and hemolysis assay. The cell viabilities of these AIEgens were over 80% at concentrations below 2×10^{-6} M and hemolytic activity was less than 5% (Figure S3, Supporting Information), thereby exhibiting good biocompatibility and facilitating their use for biological imaging. Meanwhile, for bioimaging application, the selection of appropriate excitation wavelength and acquirement of emission ranges are also crucial under the aqueous conditions of the organism. Accordingly, we tested the photophysical properties of these AIEgens in DMSO/water mixture with 99% water fraction. As shown in Figure S4 in the Supporting Information, the absorption peaks of four AIEgens were around 363 nm and the emission wavelength ranged from 430 to 700 nm. Moreover, TMTAP-7

© 2021 Wiley-VCH GmbH

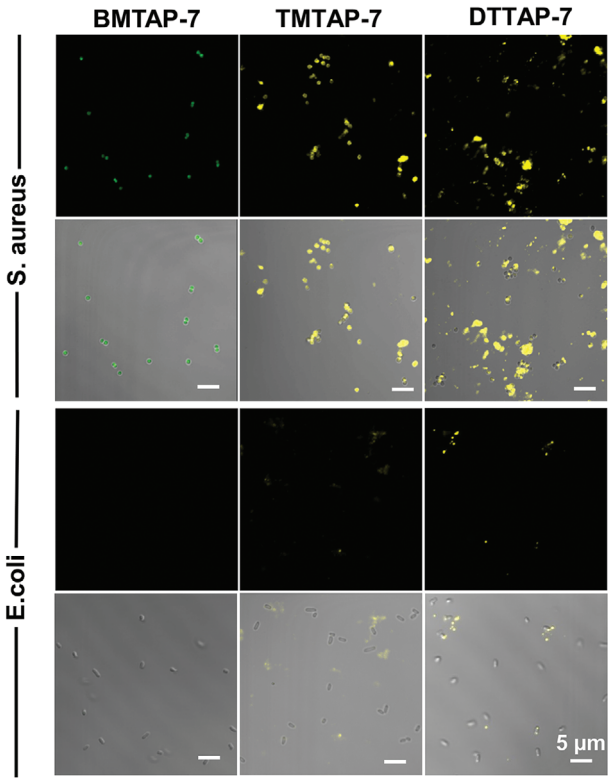

Figure 4. Fluorescence images (upper) and merged bright field and fluorescent field images (lower) of bacteria stained with BMTAP-7, TMTAP-7, and DTTAP-7 for 20 min.

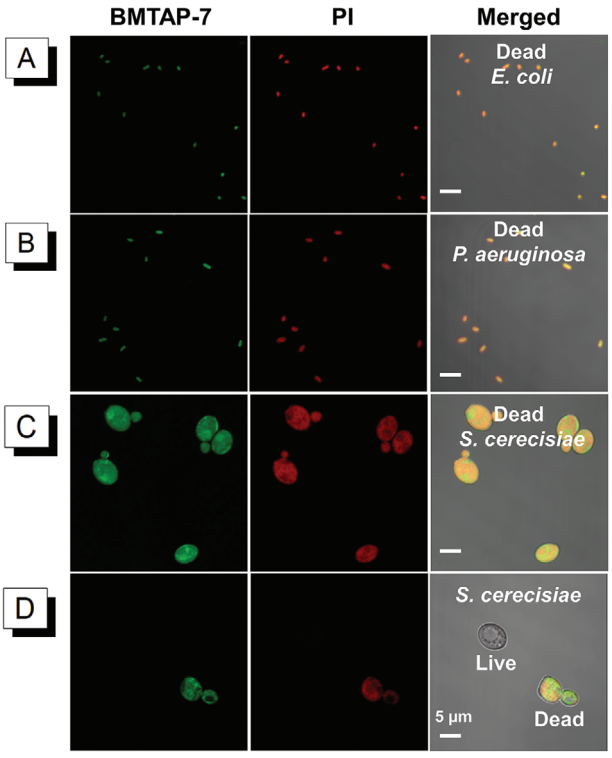

Figure 5. Fluorescence and merged images of A) dead *E. coli*, B) dead *P. aeruginosa*, C) dead *S. cerevisiae*, D) *S. cerevisiae* incubated with BMTAP-7 and PI for 20 min.

exhibited the highest quantum yield of 24.8% among them. These results facilitate the fluorescence bioimaging applications of these AIEgens.

The AIE features of BMTAP-7 and TMTAP-7 provide a direct way to visualize their entering into the cells confocal laser scanning microscopy (CLSM). Indeed, as shown in Figure S5 in the Supporting Information, BMTAP-7 could rapidly aggregate on the membrane of HeLa cells and then entered the cytoplasm with the extension of incubation time, indicating that BMTAP-7 was membrane permeable. Similar results were obtained for TMTAP-7. When it was added to the medium and incubated with HeLa cells for 30 min, its fluorescent signal also was observed inside the cells. However, fluorescence signal of DTTAP-7 in HeLa cells was only observed after incubating for 4 h (Figure S6, Supporting Information), suggesting that this compound displays a weakened ability to cross cell membranes.

To confirm the intracellular location of the AIEgens, co-localization imaging experiments were performed using MitoTracker Red (MTR), a commercial mitochondrial dye. BMTAP-7 and TMTAP-7 were highly overlapped with the MTR (Figure S6, Supporting Information), and the Pearson's correlation coefficients were as high as 0.91 and 0.93, respectively. These results could be attributed to the interactions between positively charged organic molecules and the negatively charged membrane potential of mitochondria.[19] In contrast, the Pearson's correlation coefficient for DTTAP-7 was only 0.08 (Figure S7, Supporting Information). However, this compound showed similar regional distributions in HeLa cells with the commercial lysosome dye LysoTracker® Deep Red and the Pearson's correlation coefficient of 0.63 was recorded, suggesting that DTTAP-7 might be located in the lysosome through endocytosis due to the formation of large nanoparticles. These phenomena might be closely related to the hydrophobic properties of organic molecules due to the introduction of the hydrophobic TPA moiety. To confirm this hypothesis, we estimated the theoretical Liphophilicity (ClogP) of these AIEgens by ChemBioDraw. The values of BMTAP-7, TMTAP-7, and DTTAP-7 were deduced to be 1.828, 6.439, and 11.955, respectively. High ClogP value of DTTAP-7 stands for strong hydrophobicity, which makes it enter the lysosome through endocytosis.

2.5. Selective Microbe Imaging of AIEgens

Inspired by the organelle-specific staining in HeLa cells with BMTAP-7, TMTAP-7, and DTTAP-7, we further examined whether these AIEgens could be used to selectively image microbes. First, the influence of different concentrations of BMTAP-7 on the bacteria imaging using *S. aureus* (gram-positive bacteria) as an example was explored (Figure S8A, Supporting Information). It was found that the fluorescence imaging effect at 2×10^{-6} M was lower than those at 5×10^{-6} and 10×10^{-6} M and those of 5×10^{-6} and 10×10^{-6} M are similar. Thus, the concentration of 5×10^{-6} M was selected for subsequent experiments. Afterward, a gram-negative bacteria of *Escherichia coli* (*E. coli*) was also used for comparison. As shown in **Figure 4**, after incubating

© 2021 Wiley-VCH GmbH

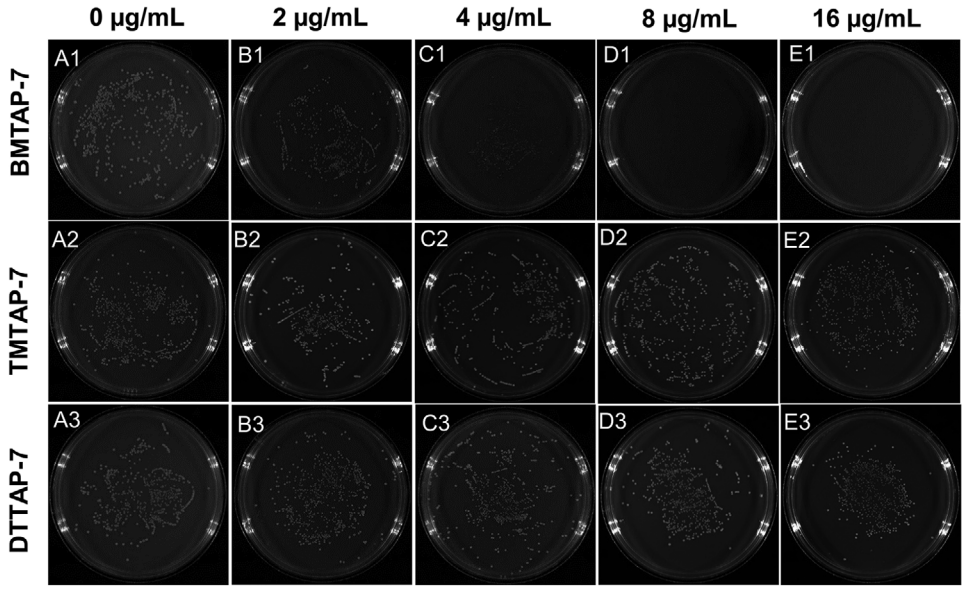

Figure 6. Bacterial inhibition tests of BMTAP-7, TMTAP-7, and DTTAP-7 in agar plates with concentrations ranging from 0 to 16 μg mL^{-1}.

Staphylococcus aureus (*S. aureus*) in PBS for 20 min, the AIEgens showed highly efficient and reliable staining even without the washing process. The hydrophilic BMTAP-7 uniformly stained every bacterium, showing a high signal-to-noise ratio over the background. For TMTAP-7 and DTTAP-7, owing to their enhanced hydrophobicity, their staining ability toward *S. aureus* decreased. In sharp contrast, we found that it was quite difficult for these AIEgens to stain *E. coli* under the same experimental conditions probably because of their multilayer outer membrane structures. These results reveal that BMTAP-7, TMTAP-7, and DTTAP-7 could be used to distinguish between *S. aureus* and *E. coli*.

It has been confirmed that the outside surfaces of gram-positive and gram-negative bacteria are negatively charged.[15] Electrostatic adsorption is the main contributor of the interaction between the cationic AIEgens and bacteria, but is not the key issue for the selective imaging behavior. We proposed that this behavior might be attributed to the bacterial outer membrane structures and permeability. Compared with the complex multilayer membrane structures of gram-negative bacteria,[15] the cell wall of gram-positive bacteria contains thick peptidoglycan and loose layer membrane, a structure that could promote the permeability of cationic AIEgens.

To verify this explanation, we used BMTAP-7 to stain dead and live *E. coli* and *Pseudomonas aeruginosa* (*P. aeruginosa*) because the membrane of dead bacteria is more permeable than those of live ones. The results showed that live bacteria could not be stained (Figure 4; Figure S8, Supporting Information), whereas the dead bacteria were thoroughly stained (**Figure 5**A,B). Afterward, we investigated whether the AIEgens could specifically discriminate different microbes. BMTAP-7 was used to stain the dead and live *S. cerevisiae*. The imaging results (Figure 5C,D) were similar to those of gram-negative bacteria. Notably, we also found that BMTAP-7 could distinguish between dead and live *S. cerevisiae* when co-stained with propidium iodide (PI). Thus, we concluded that the differences in the membrane structures of the microbes lead to the selective fluorescence imaging using these AIEgens. In addition, different from the reported cationic AIEgens, BMTAP-7 shows selective staining of Gram-positive bacteria, which may be related to the position of positive charges, amphiphilicity of the molecules (Table S1, Supporting Information).[15b]

2.6. Bacteriostatic and Mechanism Study

Owing to the unique structure of tricyclic 2-aminopyridinium derivatives and the ability to light gram-positive bacteria, we examined their bacteriostatic activity. First, the growth curves of bacteria were tested at various concentrations of BMTAP-7, TMTAP-7, and DTTAP-7 (Figure S9, Supporting Information). The results showed that they significantly inhibited *S. aureus*, but not *E. coli*. Compared with DTTAP-7, BMTAP-7 and TMTAP-7 showed effective bacteriostatic effects against *S. aureus*, possibly due to their stronger binding ability, as indicated by the fluorescence imaging. Second, we further assessed the bacteriostatic activity of these AIEgens using solid agar medium. DTTAP-7, BMTAP-7, and TMTAP-7 were added to agar plates with concentrations ranging from 0 to 16 μg mL^{-1}. After the agar plates were coated with bacteria for 24 h, we found that BMTAP-7 had a minimum inhibitory concentration (MIC) value between 4 and 8 μg mL^{-1}, which showed inhibitory bacteriostatic effects compared with TMTAP-7 and DTTAP-7 (**Figure 6**). In addition, the colony size of bacteria gradually decreased when grown with increasing concentrations of BMTAP-7 (Figure 6A1,C1).

To accurately reflect the bacteriostatic ability of BMTAP-7, TMTAP-7, and DTTAP-7, their MICs were tested in a liquid medium (i.e., nutrient broth). The MICs for BMTAP-7 and TMTAP-7 were between 4 and 8 μg mL^{-1} (**Figure 7**A), whereas DTTAP-7 showed no significant antibacterial activity. Notably, TMTAP-7 displayed significant bacteriostatic activity in liquid medium, but showed little inhibitory effects on agar plates (Figure 7B). These results might be due to the poor hydrophilicity and

© 2021 Wiley-VCH GmbH

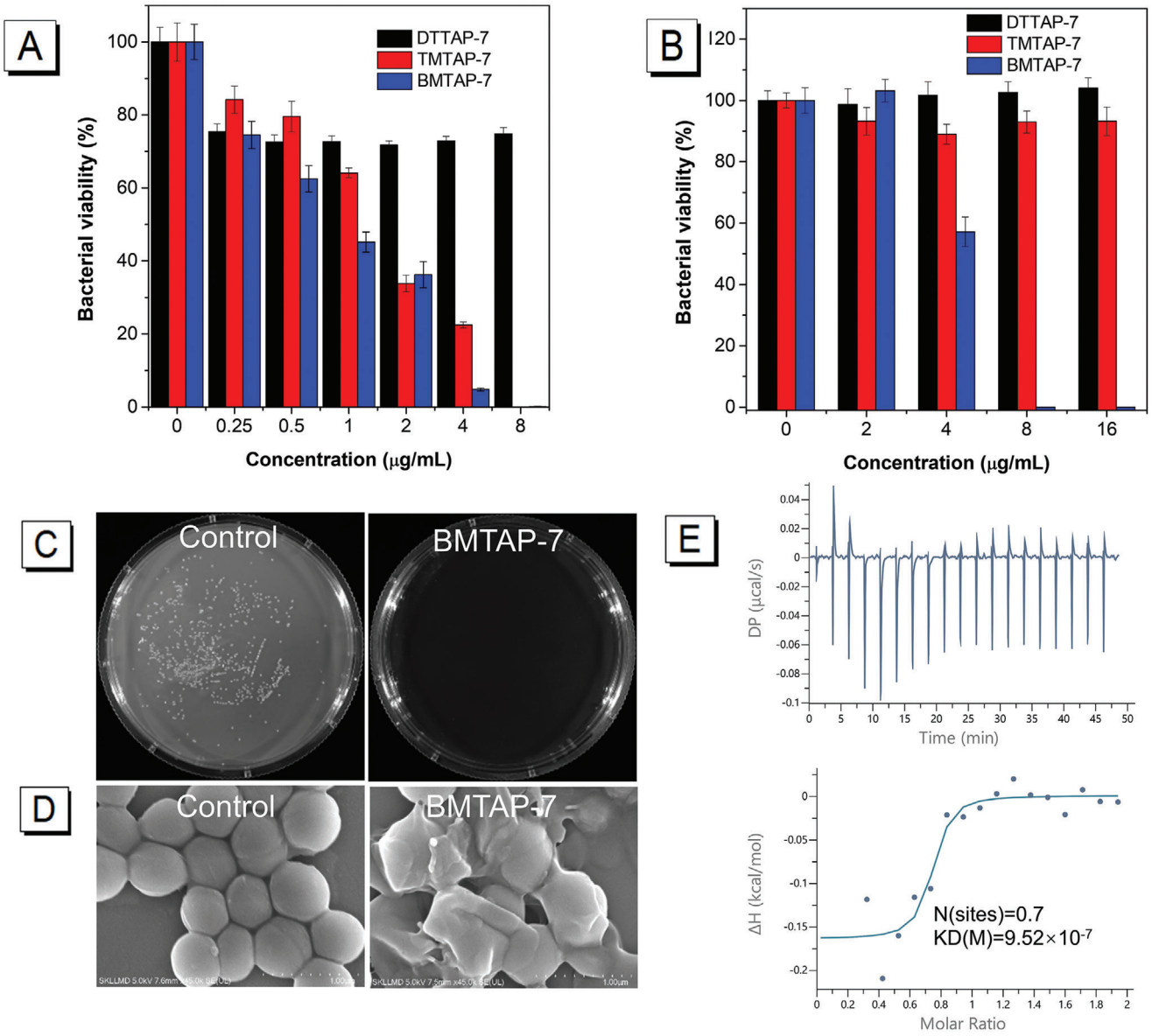

Figure 7. A) Bacteriostasis tests against *S. aureus* in nutrient broth culture or B) agar plates with different concentrations of AIEgens. C) Surface bacteriostatic experiments: BMTAP-7 and *S. aureus* were coated on the surface of the agar plates in turns. D) Morphological changes of *S. aureus* under various treatments using SEM. E) ITC results of BMTAPC-7 with lipoteichoic acid (LTA). [BMTAPC-7] = 2.0×10^{-3} M. [LTA] = 0.2×10^{-3} M.

non-uniform dispersion of the AIEgen in agar plates. To prove that the antibacterial ability of BMTAP-7 is mediated through surface contact, BMTAP-7 and *S. aureus* were coated on the surface of the agar medium in turns. As shown in Figure 7C, bacterial colonies became visible in the control group (i.e., *S. aureus* plated only), but not in the group with BMTAP-7, revealing that it could inhibit the growth of *S. aureus* through direct surface contact. It is worth noting that the MIC value of BMTAP-7 was close to the reported AIEgen and higher than those of antibiotics (Table S2, Supporting Information).

To explore the bacteriostatic mechanism of BMTAP-7 toward *S. aureus*, the morphological changes of the bacteria under various treatments were studied using scanning electron microscopy (SEM). After liquid cultures of *S. aureus* incubated with 8 μg mL^{-1} of BMTAP-7 for 24 h, we found that the outer membrane of *S. aureus* became out of shape and folded. In contrast, the *S. aureus* from the control group maintained a smooth outer membrane surface. Thus, BMTAP-7 destroyed the outer membrane of bacteria to achieve its bacteriostatic effect (Figure 7D). Furthermore, considering that bacterial growth was inhibited through surface contact based on the outer membrane surface structure, and lipoteichoic acid (LTA) is the main component in the outer membrane of *S. aureus*, the binding between BMTAPC-7 and LTA was investigated using isothermal titration calorimetry (ITC) (Figure 7E). The results showed that dissociation constants are in the same order of magnitude as the reported literature,[15a] indicating a strong binding affinity between the two components. Since no reactive oxygen species (ROS) was involved in the

© 2021 Wiley-VCH GmbH

bacteriostatic process (Figure S10, Supporting Information), we thus concluded that medium-coated BMTAP-7 could inhibit bacterial growth through electrostatic interactions with LTA on the outer membrane of *S. aureus*.

3. Conclusion

A series of AIE-active, cationic, tricyclic 2-aminopyridinium derivatives were designed and synthesized via an efficient multicomponent reaction. Investigation of the photophysical properties of BMTAPC-7 and BMTAPC-5 revealed that the RIV of seven-membered rings in the former caused the AIE effect. The increase in the hydrophobicity from BMTAP-7 to TMTAP-7, and DTTAP-7 changed the localization of them from mitochondria to lysosomes in live cells, demonstrating their efficient targeting toward organelles. Moreover, they could specifically stain gram-positive bacteria, and BMTAP-7 could distinguish between dead and live gram-negative bacteria and fungi. Specificity for imaging gram-negative bacteria and fungi was related to the structures and permeability of the outer membrane of these microbes. Furthermore, the MIC of BMTAP-7 was between 4 and 8 μg mL^{-1} for *S. aureus* in liquid and solid medium, suggesting a highly efficient bacteriostatic ability. The SEM images indicated that the damage to the outer membrane was one of the reasons for the inhibition of bacterial reproduction in liquid media. The ITC data indicated that LTA on the outer membrane of *S. aureus* could be the target of bacterial inhibition through surface contact with BMTAP-7. Collectively, this work demonstrates that the AIE-active tricyclic 2-aminopyridinium derivatives are versatile in organelle targeting and imaging, and bacterial discrimination and inhibition. Together, these derivatives potentially represent a great pharmacological tool that could be used to selectively visualize bacteriostatic processes in situ.

Supporting Information

Supporting Information is available from the Wiley Online Library or from the author.

Acknowledgements

This work was financially supported by the National Natural Science Foundation of China (Grant Nos. 21788102 and 51620105009), the Natural Science Foundation of Guangdong Province (Grant Nos. 2019B030301003 and 2016A030312002), the National Key Research and Development Program of China (Intergovernmental cooperation project, Grant No. 2017YFE0132200), and the Innovation and Technology Commission of Hong Kong (Grant No. ITC–CNERC14S01).

Conflict of Interest

The authors declare no conflict of interest.

Data Availability Statement

The data that supports the findings of this study are available in the supplementary material of this article.

Keywords

aggregation-induced emission, bacterial discrimination, bacterial inhibition, tricyclic 2-aminopyridinium derivatives

Received: January 22, 2021
Revised: April 18, 2021
Published online:

[1] N. D. Wolfe, C. P. Dunavan, J. Diamond, *Nature* **2007**, *447*, 279.
[2] X. Didelot, R. Bowden, D. J. Wilson, T. E. A. Peto, D. W. Crook, *Nat. Rev. Genet.* **2012**, *13*, 601.
[3] a) J. Zhang, Y. P. Chen, K. P. Miller, M. S. Ganewatta, M. Bam, Y. Yan, M. Nagarkatti, A. W. Decho, C. Tang, *J. Am. Chem. Soc.* **2014**, *136*, 4873. b) K. M. G. O'Connell, J. T. Hodgkinson, H. F. Sore, M. Welch, G. P. C. Salmond, D. R. Spring, *Angew. Chem., Int. Ed.* **2013**, *52*, 10706.
[4] M. Martinez-Garcia, B. K. Swan, N. J. Poulton, M. L. Gomez, D. Masland, M. E. Sieracki, R. Stepanauskas, *ISME J.* **2012**, *6*, 113.
[5] C. R. Bertozzi, M. D. Bednarski, *J. Am. Chem. Soc.* **1992**, *114*, 2242.
[6] R. J. Clifford, M. Milillo, J. Prestwood, R. Quintero, D. V. urawski, Y. I. Kwak, P. E. Waterman, E. P. Lesho, G. P. Mc, *PLoS One* **2012**, *7*, 48558.
[7] O. R. Miranda, X. Li, L. Garcia-Gonzalez, Z.-J. Zhu, B. Yan, U. H. F. Bunz, V. M. Rotello, *J. Am. Chem. Soc.* **2011**, *133*, 9650.
[8] a) A. L. Antaris, H. Chen, K. Cheng, Y. Sun, G. Hong, C. Qu, S. Diao, Z. Deng, X. Hu, B. Zhang, X. Zhang, O. K. Yaghi, Z. R. Alamparambil, X. Hong, Z. Cheng, H. Dai, *Nat. Mater.* **2016**, *15*, 235. b) A. Duarte, A. Chworos, S. F. Flagan, G. Hanrahan, G. C. Bazan, *J. Am. Chem. Soc.* **2010**, *132*, 12562. c) B. N. Giepmans, S. R. Adams, M. H. Ellisman, R. Y. Tsien, *Science* **2006**, *312*, 217. d) C. Zhu, L. Liu, Q. Yang, F. Lv, S. Wang, *Chem. Rev.* **2012**, *112*, 4687. e) H. Yuan, Z. Liu, L. Liu, F. Lv, Y. Wang, S. Wang, *Adv. Mater.* **2014**, *26*, 4333. f) H. Pei, J. Li, M. Lv, J. Wang, J. Gao, J. Lu, Y. Li, Q. Huang, J. Hu, C. Fan, *J. Am. Chem. Soc.* **2012**, *134*, 13843. g) W. Chen, Q. Li, W. Zheng, F. Hu, G. Zhang, Z. Wang, D. Zhang, X. Jiang, *Angew. Chem., Int. Ed.* **2014**, *53*, 13734. h) J. Gao, L. Li, P.-L. Ho, G. C. Mak, H. Gu, B. Xu, *Adv. Mater.* **2006**, *18*, 3145. i) H.-Y. Kwon, X. Liu, E. G. Choi, J. Y. Lee, S.-Y. Choi, J.-Y. Kim, L. Wang, S.-J. Park, B. Kim, Y.-A. Lee, J.-J. Kim, N. Y. Kang, Y.-T. Chang, *Angew. Chem., Int. Ed.* **2019**, *58*, 8426.
[9] A. B. Chinen, C. M. Guan, J. R. Ferrer, S. N. Barnaby, T. J. Merkel, C. A. Mirkin, *Chem. Rev.* **2015**, *115*, 10530.
[10] a) D. Ding, K. Li, B. Liu, B. Z. Tang, *Acc. Chem. Res.* **2013**, *46*, 2441. b) Z. Liu, H. Zou, Z. Zhao, P. Zhang, G.-G. Shan, R. T. K. Kwok, J. W. Y. Lam, L. Zheng, B. Z. Tang, *ACS Nano* **2019**, *13*, 11283.
[11] J. Mei, N. L. C. Leung, R. T. K. Kwok, J. W. Y. Lam, B. Z. Tang, *Chem. Rev.* **2015**, *115*, 11718.
[12] a) J. Mei, Y. Hong, J. W. Y. Lam, A. Qin, Y. Tang, B. Z. Tang, *Adv. Mater.* **2014**, *26*, 5429. b) S. Xie, A. Y. H. Wong, S. Chen, B. Z. Tang, *Chem. - Eur. J.* **2019**, *25*, 5824. c) E. Zhao, Y. Chen, H. Wang, S. Chen, J. W. Y. Lam, C. W. T. Leung, Y. Hong, B. Z. Tang, *ACS Appl. Mater. Interfaces* **2015**, *7*, 7180. d) X. Gu, R. T. K. Kwok, J. W. Y. Lam, B. Z. Tang, *Biomaterials* **2017**, *146*, 115. e) Q. Wan, R. Zhang, Z. Zhuang, Y. Li, Y. Huang, Z. Wang, W. Zhang, J. Hou, B. Z. Tang, *Adv. Funct. Mater.* **2020**, *30*, 2002057. f) Y. Li, Z. Zhao, J. Zhang, R. T. K. Kwok, S. Xie, R. Tang, Y. Jia, J. Yang, L. Wang, J. W. Y. Lam, W. Zheng, X. Jiang, B. Z. Tang, *Adv. Funct. Mater.* **2018**, *28*, 1804632. g) T. Zhou, R. Hu, L. Wang, Y. Qiu, G. Zhang, Q. Deng, H. Zhang, P. Yin, B. Situ, C. Zhan, A. Qin, B. Z. Tang, *Angew. Chem., Int. Ed.* **2020**, *59*, 9952. h) X. Ge, M. Gao, B. Situ, W. Feng, B. He, X. He, S. Li, Z. Ou, Y. Zhong, Y. Lin, X. Ye, X. Hu, B. Z. Tang, L. Zheng, *Mater. Chem. Front.* **2020**, *4*, 957. i) W. Zeng, Y. Xu, W. Yang, K. Liu, K. Bian, B. Zhang, *Adv. Healthcare Mater.* **2020**, *9*, 2000560. j) M. Kang, Z. Zhang, N. Song, M. Li, P. Sun, X. Chen, D. Wang, B. Z. Tang, *Aggregate* **2020**, *1*, 80.

 © 2021 Wiley-VCH GmbH

[13] a) X. Liu, M. Li, T. Han, B. Cao, Z. Qiu, Y. Li, Q. Li, Y. Hu, Z. Liu, J. W. Y. Lam, X. Hu, B. Z. Tang, *J. Am. Chem. Soc.* **2019**, *141*, 11259. b) Y. J. Li, H. T. Zhang, X. Y. Chen, P. F. Gao, C.-H. Hu, *Mater. Chem. Front.* **2019**, *3*, 1151. c) X. Chen, L. Huang, Y. Jia, R. Hu, M. Gao, L. Ren, B. Z. Tang, *Adv. Opt. Mater.* **2020**, *8*, 1902191. d) Z. Jiao, Z. Guo, X. Huang, H. Fan, M. Zhao, D. Zhou, X. Ruan, P. Zhang, S. Zhou, B. Z. Tang, *Mater. Chem. Front.* **2019**, *3*, 2647. e) D. Wang, M. M. S. Lee, G. Shan, R. T. K. Kwok, J. W. Y. Lam, H. Su, Y. Cai, B. Z. Tang, *Adv. Mater.* **2018**, *30*, 1802105. f) D. Guo, L. Li, X. Zhu, M. Heeney, J. Li, L. Dong, Q. Yu, Z. Gan, X. Gu, L. Tan, *Sci. China: Chem.* **2020**, *63*, 1198. g) C. Zhu, R. T. K. Kwok, J. W. Y. Lam, B. Z. Tang, *ACS Appl. Bio Mater.* **2018**, *1*, 1768. h) J. Yang, M. Fang, Z. Li, *Aggregate* **2020**, *1*, 6. i) B. Liu, W. He, H. Lu, K. Wang, M. Huang, R. T. K. Kwok, J. W. Y. Lam, L. Gao, J. Yang, B. Tang, *Sci. China: Chem.* **2019**, *62*, 732; J) J. Qi, C. Chen, D. Ding, B. Z. Tang, *Adv. Healthcare Mater.* **2018**, *7*, 1800477.

[14] a) T. Zhang, Y. Li, Z. Zheng, R. Ye, Y. Zhang, R. T. K. Kwok, J. W. Y. Lam, B. Z. Tang, *J. Am. Chem. Soc.* **2019**, *141*, 5612. b) G. Niu, R. Zhang, Y. Gu, J. Wang, C. Ma, R. T. K. Kwok, J. W. Y. Lam, H. H. Y. Sung, I. D. Williams, K. S. Wong, X. Yu, B. Z. Tang, *Biomaterials* **2019**, *208*, 72. c) C. Zhou, W. Xu, P. Zhang, M. Jiang, Y. Chen, R. T. K. Kwok, M. M. S. Lee, G. Shan, R. Qi, X. Zhou, J. W. Y. Lam, S. Wang, B. Z. Tang, *Adv. Funct. Mater.* **2019**, *29*, 1805986. d) Q. Hu, M. Gao, G. Feng, B. Liu, *Angew. Chem., Int. Ed.* **2014**, *53*, 14225. e) D. Wang, H. Su, R. T. K. Kwok, X. Hu, H. Zou, Q. Luo, M. M. S. Lee, W. Xu, J. W. Y. Lam, B. Z. Tang, *Chem. Sci.* **2018**, *9*, 3685.

[15] a) R. Hu, F. Zhou, T. Zhou, J. Shen, Z. Wang, Z. Zhao, A. Qin, B. Z. Tang, *Biomaterials* **2018**, *187*, 47. b) M. Kang, C. Zhou, S. Wu, B. Yu, Z. Zhang, N. Song, M. M. S. Lee, W. Xu, F.-J. Xu, D. Wang, L. Wang, B. Z. Tang, *J. Am. Chem. Soc.* **2019**, *141*, 16781. c) T. Kim, Q. Zhang, J. Li, L. Zhang, J. V. Jokerst, *ACS Nano* **2018**, *12*, 5615. d) K. P. Prasad, A. Than, N. Li, M. Alam Sk, H. Duan, K. Pu, X. Zheng, P. Chen, *Mater. Chem. Front.* **2017**, *1*, 152. e) P. Prasad, A. Gupta, P. K. Sasmal, *Chem. Commun.* **2021**, *57*, 174. f) X. Feng, B. Tong, J. Shi, C. Zhao, Z. Cai, Y. Dong, *Mater. Chem. Front.* **2021**, *5*, 1164.

[16] F. Bu, R. Duan, Y. Xie, Y. Yi, Q. Peng, R. Hu, A. Qin, Z. Zhao, B. Z. Tang, *Angew. Chem.* **2015**, *127*, 14700; *Angew. Chem., Int. Ed.* **2015**, *54*, 14492.

[17] O. Bakulina, F. K. Merkt, T.-O. Knedel, C. Janiak, T. J. J. Müller, *Angew. Chem.* **2018**, *130*, 17486; *Angew. Chem., Int. Ed.* **2018**, *57*, 17240.

[18] M. M. S. Lee, W. Xu, L. Zheng, B. Yu, A. C. S. Leung, R. T. K. Kwok, J. W. Y. Lam, F.-J. Xu, D. Wang, B. Z. Tang, *Biomaterials* **2020**, *230*, 119582.

[19] a) H. Huang, L. Yang, P. Zhang, K. Qiu, J. Huang, Y. Chen, J. Diao, J. Liu, L. Ji, J. Long, H. Chao, *Biomaterials* **2016**, *83*, 321. b) J. Zielonka, J. Joseph, A. Sikora, M. Hardy, O. Ouari, J. Vasquez-Vivar, G. Cheng, M. Lopez, B. Kalyanaraman, *Chem. Rev.* **2017**, *117*, 10043.

© 2021 Wiley-VCH GmbH